Published in final edited form as:
Neuron. 2013 October 16; 80(2): . doi:10.1016/j.neuron.2013.08.013.

Deficiency of asparagine synthetase causes congenital microcephaly and a progressive form of encephalopathy

Elizabeth K. Ruzzo[1,25], **José-Mario Capo-Chichi**[2,25], **Bruria Ben-Zeev**[3,4,25], **David Chitayat**[5,6], **Hanqian Mao**[8], **Andrea L. Pappas**[7], **Yuki Hitomi**[1], **Yi-Fan Lu**[1], **Xiaodi Yao**[1], **Fadi F. Hamdan**[2], **Kimberly Pelak**[1], **Haike Reznik-Wolf**[4,9], **Ifat Bar-Joseph**[3,4,9], **Danit Oz-Levi**[10], **Dorit Lev**[4,11,12], **Tally Lerman-Sagie**[4,12,13], **Esther Leshinsky-Silver**[4,12,14], **Yair Anikster**[3,4], **Edna Ben-Asher**[10], **Tsviya Olender**[10], **Laurence Colleaux**[15], **Jean-Claude Décarie**[16], **Susan Blaser**[17], **Brenda Banwell**[18], **Rasesh B. Joshi**[7], **Xiao-Ping He**[7], **Lysanne Patry**[2], **Rachel J. Silver**[6], **Sylvia Dobrzeniecka**[19], **Mohammad S. Islam**[20], **Abul Hasnat**[20], **Mark E. Samuels**[2], **Dipendra K. Aryal**[21], **Ramona M. Rodriguiz**[21], **Yong-hui Jiang**[22], **William C. Wetsel**[21,23], **James O. McNamara**[7], **Guy A. Rouleau**[19,24], **Debra L. Silver**[8], **Doron Lancet**[10], **Elon Pras**[3,9], **Grant A. Mitchell**[2], **Jacques L. Michaud**[2,26], and **David B. Goldstein**[1,26]

[1]Center for Human Genome Variation, Duke University School of Medicine, Durham, North Carolina, 27708, USA

[2]Sainte-Justine Hospital Research Center, Montreal, Quebec, Canada, H3T 1C5

[3]Edmond and Lily Safra Children's Hospital, Sheba Medical Center, Ramat Gan, Israel

[4]The Sackler School of Medicine, Tel Aviv University, Tel Aviv, Israel

[5]The Hospital for Sick Children, Division of Clinical and Metabolic Genetics, UoT, Toronto, Ontario, Canada, M5G 2L3

[6]Mount Sinai Hospital, The Prenatal Diagnosis and Medical Genetics Program, UoT, Toronto, Ontario, Canada, M5G 1Z5

[7]Department of Neurobiology, Duke University, Durham, North Carolina, 27708, USA

[8]Molecular Genetics and Microbiology and The Duke Institute for Brain Sciences, Duke University, Durham, North Carolina, 27708, USA

[9]The Danek Gertner Institute of Human Genetics, Sheba Medical Center, Ramat Gan, Israel

[10]Department of Molecular Genetics, Weizmann Institute of Science, Rehovot, 76100, Israel

[11]Institute of Medical Genetics, Wolfson Medical Center, Holon, 58100, Israel

[12]Metabolic Neurogenetic Clinic, Wolfson Medical Center, Holon, 58100, Israel

[13]Pediatric Neurology Unit, Wolfson Medical Center, 58100 Holon, Israel

*Correspondence: David B. Goldstein (d.goldstein@duke.edu) and Jacques L. Michaud (jacques.michaud@recherche-ste-justine.qc.ca).
[25]These authors contributed equally to this work.
[26]These authors jointly directed this work.

SUPPLEMENTAL INFORMATION

Supplemental Information includes additional experimental procedures, including detailed phenotypic information on these patients, as well as five gures and 11 tables.

[14]Molecular Genetics Laboratory, Wolfson Medical Center, Holon, 58100, Israel

[15]Hôpital Necker-Enfants Malades, 75015 Paris, France

[16]Department of Medical Imaging, Sainte-Justine Hospital, Montreal, Quebec, Canada, H3T 1C5

[17]Department of Medical Imaging, The Hospital for Sick Children, UoT, Toronto, Ontario, Canada, M5G 2L3

[18]Division of Neurology, The Children's Hospital of Philadelphia, Philadelphia, PA

[19]Research Center, Centre Hospitalier de l'Universite de Montreal, Montreal, Québec, Canada, H2L 2W5

[20]Department of Clinical Pharmacy & Pharmacology, Faculty of Pharmacy, University of Dhaka, Dhaka, 1000, Bangladesh

[21]Department of Psychiatry and Behavioral Sciences, Mouse Behavioral and Neuroendocrine Analysis Core Facility, Duke University, Durham, North Carolina, 27710, USA

[22]Department of Pediatrics and Neurobiology, Duke University School of Medicine, Durham, North Carolina 27710, USA

[23]Department of Cell Biology and Neurobiology, Duke University, Durham, North Carolina, 27710, USA

[24]Montreal Neurological Institute, McGill University, Montreal, Quebec, Canada, H3A 2B4

SUMMARY

We analyzed four families that presented with a similar condition characterized by congenital microcephaly, intellectual disability, progressive cerebral atrophy and intractable seizures. We show that recessive mutations in the *ASNS* gene are responsible for this syndrome. Two of the identified missense mutations dramatically reduce ASNS protein abundance, suggesting that the mutations cause loss of function. Hypomorphic *Asns* mutant mice have structural brain abnormalities, including enlarged ventricles and reduced cortical thickness, and show deficits in learning and memory mimicking aspects of the patient phenotype. *ASNS* encodes asparagine synthetase, which catalyzes the synthesis of asparagine from glutamine and aspartate. The neurological impairment resulting from *ASNS* deficiency may be explained by asparagine depletion in the brain, or by accumulation of aspartate/glutamate leading to enhanced excitability and neuronal damage. Our study thus indicates that asparagine synthesis is essential for the development and function of the brain but not for that of other organs.

INTRODUCTION

Intellectual disability (ID) affects 2–3% of the general population and is characterized by a broad range of cognitive deficits. It is usually subdivided into syndromic and nonsyndromic forms, depending on whether additional abnormalities are found. Syndromic ID is often accompanied by microcephaly, defined by a head circumference more than two standard deviations (SD) below the age- and sex-adjusted mean. The incidence of microcephaly, as reported in birth defect registries world-wide, varies from 1 to 150 per 100,000 depending upon the range of SD used to define microcephaly and the ethnic population. For example, microcephaly is more prevalent in populations with a high degree of consanguinity(Mahmood et al., 2011). Causes of congenital microcephaly include metabolic disorders, chromosomal anomalies, and intra-uterine infections. However, with the exception of autosomal recessive primary microcephaly (MCPH), the genetic etiology of most congenital microcephaly cases is unknown.

We ascertained four families with a distinct form of severe encephalopathy associated with congenital microcephaly and progressive brain atrophy. Two families were from the same ethnic group whereas the other two families were independently recognized as presenting with an identical syndrome. Both pairs of families were analyzed independently by exome sequencing. Here we report the clinical features of the affected children and demonstrate that the observed phenotype in all four families can be explained by autosomal recessive deficiency of asparagine synthetase (ASNS).

RESULTS

Identification and validation of *ASNS* mutations

We identified a total of nine children from four families with a severe form of intellectual disability (Table 1; Figure 1A; Supplemental Experimental Procedures). These children were born with a small head circumference and showed progressive microcephaly. Although congenital microcephaly is a consistent feature of this syndrome, the patients do not fit the definition of primary microcephaly (MCPH) (Supplemental Experimental Procedures). Their clinical course was characterized by profound developmental delay and, in a majority of cases, early-onset intractable seizures (Table 1, Figure 2, Figure S1). Clinical examination revealed axial hypotonia with severe appendicular spasticity in all cases. All affected siblings of family C also showed excessive startle reflex, mimicking hyperekplexia. In addition, several affected individuals from families C and D had episodes of hypothermia. Brain MRI first performed in early infancy showed decreased cerebral volume and size of pons, presumably caused by hypodevelopment and/or atrophy, as well as delayed myelination (Figure 2; Figure S1). Some patients also showed gyral simplification. The affected children from two families (C and D) died during the first year of life because of pulmonary aspiration secondary to severe neurological dysfunction, whereas the affected individuals from the other families survived into their third decade.

Families A and B are unrelated but are both of Iranian Jewish ancestry. Targeted exonic regions were captured and sequenced in one affected individual from family A (A.II.1) and two from family B (B.II.2 and B.II.4). We focused on variants that were annotated as having a plausible impact on the function of the resulting gene product (e.g., missense, nonsense, splice site, intron-exon boundary, and coding-disrupting indels). We compared patient exomes to control exomes sequenced in the same facility (n=261, unrelated samples, not enriched for neurological disorders). Because families A and B belong to the same ethnic community and were the only similar cases identified in Israel to date, we postulated that the causal variant would be a founder mutation in this population shared amongst all affected individuals in these families. We therefore first focused on homozygous variants that were shared by both siblings in family B (Figure 1A, B.II.2 and B.II.4) and that were uncommon in our control population (Table S1). Since the incidence of this disorder is very low in the general population, we inspected only variants with a predicted frequency of ≤3% in our sequenced control genomes. We found 72 such variants, only three of which were absent in the control population (Table S2). Furthermore, only one of these three variants was also present in homozygous form in the patient from family A (Figure 1A, A.II.1). This variant, located in the asparagine synthetase (*ASNS*) gene, causes a missense change (c.1084T>G) resulting in a phenylalanine to valine substitution at amino acid position 362 (p.F362V; NM_183356). We also performed homozygosity mapping. We found p.F362V lies in the largest homozygous region and found no additional candidates of interest in the homozygous regions (Supplemental Experimental Procedures, Tables S7–S9).

Family C is composed of three affected (C.II.1, C.II.3 and C.II.4) siblings and one healthy (C.II.2) sibling born to consanguineous parents of Bangladeshi origin (Figure 1A). No DNA was available for the first affected child (C.II.1) who had the same clinical manifestations as

his affected brothers. Homozygosity mapping showed that the two affected siblings share a total of eight homozygous regions that are >1 Mb in size (Table S3). Exome sequencing performed in one of the affected children (C.II.3) identified 856 rare protein or splice-altering variants (with a frequency ≤3% in 169 in-house unrelated exomes, 1,000 Genomes Project data-set and data from the National Heart, Lung, and Blood Institute (NHLBI) Exome Sequencing Project (ESP)). These included three variants that map to the shared regions of homozygosity; the three variants were Sanger sequenced and all three variants were homozygous in both affected individuals. The parents and the unaffected sibling were heterozygous for two of these variants, whereas the other candidate variant was excluded from further consideration because it was found in a homozygous form in one of the parents. One of the remaining variants, c.1282G>A (p.D428N; NM_017460) in the *CYP3A4* gene, is not predicted to affect protein function by SIFT or Polyphen-2(Adzhubei et al., 2010; Ng and Henikoff, 2003) and *CYP3A4* encodes a component of cytochrome P450 (subfamily 3A, polypeptide 4), which is predominantly expressed in the liver. Thus, the *CYP3A4* variant seemed unlikely to be responsible for this phenotype. The sole remaining variant in this family is c.1648C>T (p.R550C; NM_183356) in *ASNS*, which is present in the largest region of homozygosity (35 Mb) shared by the two affected children (Table S4).

Family D is a non-consanguineous French Canadian family, consisting of three affected (D:II.1, II.2, and II.3) and two unaffected siblings (D:II.4 and II.5) (Figure 1A). Exome sequencing was performed in two affected (D:II.1 and II.2) and two unaffected siblings. In total, 237 rare protein or splice-altering variants were present in both affected children (with a frequency ≤3% in 169 in-house unrelated exomes, 1,000 Genomes Project data-set and data from the NHLBI ESP). We excluded from this list X-linked variants that were also present in the unaffected male sibling. We also excluded homozygous or possible compound heterozygous variants that were found in the same form in at least one unaffected sibling. Only two variants (c.1648C>T/p.R550C; c.17C>A/p.A6E; NM_183356), both in *ASNS*, remained after this filtering process (Table S5).

Critically, in all four families there is complete cosegregation of the identified *ASNS* mutations/genotypes with disease (Figure 1A). Sanger sequencing was used to validate all three mutations (Figure 1B).

All three missense mutations are predicted to damage the encoded asparagine synthetase protein by available computer algorithms (SIFT and PolyPhen-2) and all three mutations are absent in dbSNP135, the 1,000 Genomes Project data-set and data from the NHLBI ESP (Table 2). To better estimate the frequency of the p.F362V variant in unaffected individuals, we directly genotyped this locus in 1,160 additional controls and failed to detect the mutation. Finally, all three mutations were genotyped in ancestry-matched controls and all remained absent (Table 2), with the exception of p.F362V which has an estimated carrier frequency of 0.0125 in Iranian Jews.

Additionally, we used the sequence data to test for evidence of cryptic relatedness between the patient in family A and the affected siblings from family B, and found no indication of elevated identity by descent beyond what is expected for unrelated genomes (data not shown). We also tested whether the p.F362V *ASNS* variant is found on a common haplotype in all affected individuals of Iranian Jewish origin. Indeed, the *ASNS* variant was found on the same 1.2 Mb haplotype in both families and this haplotype was very rare (0.8%) in 261 sequenced controls (Supplemental Experimental Procedures; Table S6). This observation is consistent with a single founder origin for p.F362V and subsequent transmission along with the same extended haplotype. We also did not find evidence for homozygote deletions overlapping the *ASNS* gene in controls (Supplemental Experimental Procedures).

Interestingly, the mutation p.R550C was found in two families of different ethnic backgrounds. This mutation was associated with different haplotypes in each of these families, suggesting that it arose independently. It should be noted that p.R550C corresponds to a CpG site, which is associated with a higher mutation rate(Nachman and Crowell, 2000), possibly explaining the recurrence of this rare mutation in different populations.

Functional impact of the nonsynonymous mutations

To test the effect of the identified mutations on ASNS RNA and protein levels, we generated full-length mutant cDNA constructs (p.A6E, p.F362V, and p.R550C) using PCR-directed mutagenesis (Figure S2). We then transfected both wild-type and mutant alleles into HEK-293 and COS-7 cells and found similarly robust levels of expression of the mRNA corresponding to wild-type and all three mutant alleles (Figure 3A). This result indicates that these mutations do not overtly affect RNA levels, suggesting they do not influence RNA stability. For the p.F362V mutation, we also compared wild-type and mutant full-length transcripts, from the patient fibroblasts, to detect any differences in alternative splicing or exon skipping, and found no evidence for alternately spliced transcripts (data not shown).

We used two approaches to detect the ASNS protein in transfected cells. We used an anti-human ASNS antibody (Figure S2). This antibody cross-reacted with some non-specific bands and thus we also used C-terminal FLAG-tagged forms of ASNS to detect the wild-type and all three mutant forms of ASNS (Figure S2) using the anti-FLAG antibody. We found that while high levels of the wild-type protein were easily detected, a dramatic reduction in protein abundance was seen in the HEK-293 cells expressing the p.A6E or p.F362V mutant allele. In contrast, cells expressing the p.R550C mutant allele had an increased level of protein abundance compared to wild type (Figure 3B). Consistent with the former observation, a dramatic reduction in ASNS abundance was observed in patient fibroblasts from individual II.1 in Family A, harboring the p.F362V allele (Figure S2). This pattern of protein abundance was also observed in COS-7 cells transfected with empty, wild-type, or mutant vectors (Figure S2). These results suggest that these mutations impaired *ASNS* gene function by either reducing protein expression (p.A6E or p.F362V) or reducing functional performance (p.R550C). The mechanism through which the R550C mutation reduces activity remains to be elucidated, but the clinical similarity in presentation of patients suggests that all mutations are loss of function mutations.

We then asked whether these mutations destabilize the protein, targeting it for degradation. We blocked both the ubiquitin-proteasome and the macroautophagy pathways, but neither of these altered ASNS protein abundance (data not shown). We also used Leupeptin to inhibit lysosomal-dependent degradation and this also failed to rescue the p.A6E or p.F362V mutant proteins to wild-type levels (Figure 3B), although some experiments did show a trend toward rescue (data not shown).

ASNS encodes the glutamine-dependent asparagine synthetase enzyme (EC 6.3.5.4), which catalyzes ammonia transfer from glutamine to aspartic acid via a β-aspartyl-AMP intermediate. Concordant with this biochemical function, we found that the levels of asparagine were decreased in at least two affected individuals (C.II.3 and D.II.1) whereas glutamine and aspartic acid, both precursors in the ASNS-catalyzed synthesis of asparagine, were mildly elevated in the patients from family B (Table 3). These findings are consistent with our *in vitro* functional studies, emphasizing that the identified mutations have phenotypic consequences.

The mutated amino acid residues in ASNS are located within regions of high sequence conservation among orthologs, from bacterium to man (Figure 4A), indicating that these amino acids are likely to be critical for protein function. This is further supported by the

inferred positions of the human ASNS mutations in the folded bacterial ortholog (Figure 4B; Supplemental Experimental Procedures).

ASNS expression in the brain

Cells are capable of both nutritional intake and endogenous synthesis of asparagine, suggesting that ASNS may be dispensable, and raising the question of how loss of ASNS protein or its dysfunction results in a severe, tissue-specific phenotype. *ASNS* is under complex transcriptional regulation(Chen, 2004; Greco et al., 1989; Li et al., 2006; Richards and Kilberg, 2006) and is expressed at low levels in most tissues, but is highly expressed in the adult brain, with evidence for a brain-specific splice variant(s) (Figure S3)(Hongo et al., 1996). Consistent with this expression pattern, *Asns* is expressed in the adult mouse brain (Allen Brain Atlas). *In situ* hybridization shows that *Asns* is also expressed in the developing embryonic mouse brain (E14.5), and is particularly enriched in the cortical plate where the neurons reside, and is also expressed in the ventricular and sub-ventricular zone layers (VZ and SVZ) lining the ventricles of the cerebral cortex, where neural progenitors reside (Figure S3)(Visel et al., 2004). RNA-seq of E14.5 cortices also confirms this pattern of expression in the cortical plate and VZ(Ayoub et al., 2011). This expression pattern is similar to that of known microcephaly genes(Bond et al., 2002; Jackson et al., 2002), consistent with a role for *Asns* in cortical development and brain size.

Asns gene-trap mice

We obtained genetically modified mice from EUCOMM in which the *Asns* genomic locus contains a gene-trap insertion in intron 2 (ENSMUST00000115542) containing a splice acceptor site and the LacZ gene (B6NTac;B6N-Asns$^{tm1a(EUCOMM)Wtsi}$/H, termed *Asns*$^{-/-}$; Figure S4).

Gene-traps are frequently hypomorphs, as there can be splicing that skips over the gene-trap cassette, but the degree to which this splicing occurs is construct and gene specific(Adams and van der Weyden, 2008). To determine the extent of *Asns* expression in the *Asns* gene-trap mice, we performed a comprehensive *Asns* mRNA analysis in the brains (cerebral hemispheres) of adult *Asns*$^{+/+}$, *Asns*$^{+/-}$, and *Asns*$^{-/-}$ mice (three to four months of age). First, RT-PCR was used to semi-quantitatively assess the existence of *Asns* mRNA transcripts. RT-PCR spanning from the second exon to the last exon (exon 12) revealed a single band the size of the expected wild-type *Asns* transcript in all three genotypes (Figure S4). These bands were gel purified and Sanger sequenced, which confirmed the wild-type transcript was present in all three genotypes and no aberrant splicing events were observed. Additionally, *Gapdh* RT-PCR was performed as an internal control and the homozygous mice show a decreased abundance of the wild-type *Asns* transcript compared to the wild type mice (Figure S4). To quantify this difference, we performed quantitative real-time TaqMan PCR using a probe spanning exons seven and eight. The mRNA levels were significantly different between the three genotypes (one-way analysis of variance (ANOVA); $P<0.00001$) (Figure 5A). A post-hoc two-tailed t-test revealed both mutant genotypes were significantly different from wild type mRNA levels ($P_{WT\text{-}Asns(+/-)}=0.00001$, $*P_{WT\text{-}Asns(-/-)}<0.00001$) and significantly different from each other ($*P_{Asns\ (+/-)\text{-}Asns(-/-)}=0.00083$). We were unable to determine if there was differential expression of the Asns protein, due to lack of quality and specific mouse anti-Asns antibodies. These data demonstrate that the *Asns* gene-trap mouse is a hypomorph with ~20% of the normal level of *Asns* mRNA being expressed. Given that two of the human mutations lead to decreased protein expression, this mouse provides a reliable model for this phenotype.

We next analyzed the brains of *Asns*$^{-/-}$ and control (*Asns*$^{+/+}$ *or Asns*$^{+/-}$) littermates from embryos and adults. We obtained coronal sections from postnatal day (P) zero brains and measured cortical area, cortical thickness, and lateral ventricle area for each mouse using rostral-caudal matched sections (using anatomical landmarks). We found that the cortical thickness and area of the *Asns*$^{-/-}$ brains were on average, ~14% thinner and ~5% smaller than their control littermates, respectively. Additionally, the lateral ventricle area in the *Asns*$^{-/-}$ mice was significantly larger than their control littermates (P=0.019, Figure S4).

Due to the progressive nature of the human disorder, we next evaluated whether adults showed exacerbated brain defects. We generated paraffin embedded coronal sections from P84 brains of homozygous *Asns*$^{-/-}$ and heterozygous *Asns*$^{+/-}$ littermates (three of each genotype) (representative sections shown in Figure S4). The use of heterozygous animals was considered suitable because human carriers of *ASNS* mutations remain unaffected. We analyzed rostral-caudal matched sections (using anatomical landmarks) from each animal for several parameters. Measurement of the cortical surface area, using methods described by Pulvers and colleagues (Pulvers et al., 2010), showed an ~8% reduction in cortical surface area of *Asns*$^{-/-}$ mice (Figure 5B). A similar reduction (~5%) was observed in the whole brain surface area of *Asns*$^{-/-}$ mice (Figure 5C). We also observed that the *Asns*$^{-/-}$ brains had increased lateral ventricles (~95%) relative to control brains (Figure 5D). Importantly, the cortical thickness of the *Asns*$^{-/-}$ mice was significantly reduced compared to the *Asns*$^{+/-}$ mice (P=0.022, Figure 5E).

Asns$^{+/-}$ and *Asns*$^{-/-}$ mice were assessed with age-matched B6NTac control animals in four behavioral assays. We found no genotype-associated differences in spontaneous locomotor activity, performance on the rotorod, or anxiety-like behavior in the light-dark emergence test; however, *Asns*$^{+/-}$ mice were deficient and *Asns*$^{-/-}$ mice were severely impaired in short- and long-term memory in the novel object recognition task (Supplemental Experimental Procedures, Figure S5).

Careful observations of mice during behavioral testing revealed no evidence of seizure activity. To examine the possibility that *Asns*$^{-/-}$ mice might display epileptiform activity, prolonged video-EEG recordings were conducted in chronically implanted *Asns*$^{-/-}$ mice (n=2) and *a WT* control (n=1). Neither behavioral nor electrographic seizures were detected in *Asns*$^{-/-}$ mice or the *WT* controls.

Taken together these data indicate that this Asns mouse model recapitulates the human brain phenotype, particularly in the reduced cortical thickness and increased lateral ventricle area.

DISCUSSION

We report that mutations in asparagine synthetase (*ASNS*) cause a novel neurodevelopmental disorder characterized by congenital microcephaly, profound intellectual disability, and progressive cerebral atrophy. We found that two of these mutations reduce the abundance of the protein. Finally, we have shown that disrupting this gene in mice creates a model that mimics aspects of the human phenotype, including structural brain abnormalities and learning deficits, albeit with what appears to be a generally milder presentation than observed in humans.

Studies performed on cancer cells showed that asparagine depletion affects cell proliferation and survival (reviewed in Richards and Kilberg, 2006). This is classically illustrated by the effect of asparaginase administration in childhood acute lymphoblastic leukemia, which is characterized by low asparagine synthetase levels. Asparaginase delivery to the bloodstream results in asparagine depletion causing a rapid efflux of cellular asparagine, which is also destroyed. Most cells express sufficient ASNS to counteract this asparagine starvation and

survive, but not leukemic cells. Similarly, loss of ASNS activity in thermosensitive mutant BHK cells leads to cell cycle arrest as a consequence of a depletion of cellular asparagine (Greco et al., 1989; Li et al., 2006).

During development *Asns* is expressed in regions where both neural progenitors and post-mitotic neurons are present, suggesting it may function in either or both of these populations. A subset of the brains from our subjects had simplified gyri. Similar features were found in the mutant mice, which showed decreased cortical thickness and enlarged lateral ventricles. These structural abnormalities could be caused in part by aberrations in neural progenitor proliferation during development, resulting from decreased asparagine levels. Asparagine depletion could also cause increased cell death in post-mitotic neurons or glial cells, contributing to the progressive atrophy of the brain observed in our subjects.

Strikingly, ASNS deficiency causes severe neurological impairment, without any involvement of peripheral tissues. The concentration of asparagine in the CSF of humans is only ~10% of the concentration found in plasma(Scholl-Burgi et al., 2008a). The poor transport of asparagine across the blood-brain barrier suggests that the brain depends on local *de novo* synthesis, explaining why the phenotype is essentially neurological.

In addition to ID, a subset of our patients presented with features of hyper-excitability (including epilepsy and hyperekplexia). These features suggest a mechanism that is consistent with the accumulation of aspartate/glutamate in the brain, resulting in enhanced excitability and neuronal damage. While seizures in the patients could reflect enhanced excitability, these could also be secondary to the structural effects of altered proliferation. We cannot exclude the possibility that multiple mechanisms may be contributing to the observed human phenotype. Further analyses of animal and cellular models will help to elucidate the function of ASNS for normal brain development.

Of particular interest is the observation that *Asns* hypomorphic mice appear to have a milder phenotype than the humans with regards to more modest structural effects on the brain and no evidence of seizures. The ratio for the concentration of asparagine in the cerebrospinal fluid (CSF) to plasma in rats (0.26)(Nishimura et al., 1995) appears to be slightly elevated compared to that of humans (0.081(Akiyama et al., 2012) to 0.118(Scholl-Burgi et al., 2008b)). Assuming the CSF/plasma ratio is similar in mouse and rat, this suggests that the concentration of asparagine is increased in the CSF and interstitial fluid (ISF) of mouse/rat as compared to humans. Thus, asparagine may be more readily available to the $Asns^{-/-}$ mice due to some physiological difference between humans and mice, such as transport at the blood-brain barrier. Alternately, it is possible that low levels of *Asns* expression in these mice result in a less severe phenotype. It will be of great interest to compare the hypomorph to a complete *Asns* null animal, which may show an even more dramatic phenotype.

With this report, ASNS deficiency becomes the third example of a recently-recognized group of conditions, all of which feature severe congenital encephalopathy with microcephaly. These conditions each result from the inability to synthesize a nonessential amino acid. The others are glutamine synthetase deficiency(Häberle et al., 2013) and the serine biosynthetic disorders(de Koning, 2013). Although knowledge of ASNS deficiency and of other inborn errors of nonessential amino acid synthesis is incomplete, general considerations regarding diagnosis, disease mechanism and treatment are in order. In almost every respect, the clinical approach to these diseases is predicted to be the opposite of that recommended for classical aminoacidopathies, which are caused by deficient breakdown of essential amino acids.

Strikingly, every diagnosis of ASNS deficiency was made by molecular genetics, despite extensive previous evaluation of patients that in several cases included amino acid

chromatography of plasma and CSF. Why was ASNS deficiency not suspected on these grounds? The answer may lie in a combination of technical considerations and biology. Compared to most amino acids, the normal levels of asparagine are low, both in plasma (e.g., 50.7 ± 17.7 μmol/L, in children 0–3 years old) and CSF (e.g., 4.0 ± 2.9 μmol/L) (Akiyama et al., 2012; Scholl-Burgi et al., 2008a). For many reasons, low levels of a metabolite may be less evident than increases. Abnormally low levels are more easily concealed by variations due to physiological state such as nutrition (which is difficult to standardize in ill newborns or infants) and to machine performance in diagnostic laboratories. In fact, currently used diagnostic technologies cannot discriminate low from normal CSF asparagine levels. In summary, results to date suggest that in patients with unexplained congenital encephalopathy with microcephaly, the absence of a low value does not exclude ASNS deficiency. In the future, an enzyme assay may play an important role in the complete diagnostic evaluation of patients suspected of ASNS deficiency but experience is too limited to conclude. In children with severe congenital encephalopathy and microcephaly, ASNS deficiency should be considered, and molecular diagnosis is the only method with proven reliability.

All three known deficiencies of amino acid biosynthesis present mainly with neurological features. In these conditions, the deficient amino acid becomes essential. Hence, a logical first consideration for therapy is dietary supplementation, to provide the deficient amino acid to the brain. Plasma levels can usually be substantially increased by dietary supplementation and despite the complex transport systems for amino acids at the brain endothelium, a therapeutic benefit of supplementation has been reported in serine biosynthetic disorders and glutamine synthetase deficiency(de Koning, 2013; Häberle et al., 2012). Supplementation with asparagine therefore seems reasonable in ASNS deficiency. However, the prenatal onset of the microcephaly and the early postnatal presentation raise the possibility that such treatment will not be curative unless started prenatally.

The *Asns* mouse we have analyzed here will provide a model for future comprehensive exploration of the factors influencing phenotypic severity. Comparing this hypomorphic mouse model with a null mouse model will enable evaluations of the efficacy of dietary interventions, which will be critical information for assessment of possible dietary therapies. This work therefore sets the stage for evaluation of treatment options in *Asns* mouse models.

Early diagnosis of ASNS deficiency is now possible. Careful clinical observations and studies of Asns-deficient mice will help define the clinical spectrum and resolve central unanswered issues regarding the pathophysiology of this condition.

EXPERIMENTAL PROCEDURES

Recruitment of subjects and collection of samples

Families A and B were recruited at Sheba and Wolfson Medical Centers in Israel, family C at The Hospital for Sick Children in Toronto (Canada) and family D at Sainte-Justine Hospital in Montreal (Canada). Blood samples were obtained from most affected individuals, their unaffected siblings and their parents. The relevant Institutional Review Boards approved the studies and appropriate family members gave written consent.

Sequencing and variant identification

Exome sequencing in families A & B—The Illumina Genome Analyzer IIx platform (Illumina, Inc. San Diego, CA) was used to perform exome-sequencing of the three sequenced microcephaly patients (Figure 1, Family A: II-1 & Family B: II-2, II-4) at the Center for Human Genome Variation (CHGV) at Duke University, Durham, North Carolina.

Prior to sequencing, target regions were captured using the SureSelect Human All Exon technology (Aligent Technologies, Santa Clara, CA). This technology captures CCDS exonic regions and flanking intronic regions totaling ~38Mb of genomic DNA. The resulting short-sequence reads were aligned to the reference genome (NCBI human genome assembly build 36; Ensembl core database release 50_361(Hubbard et al., 2009)) using the Burrows-Wheeler Alignment (BWA) tool(Li and Durbin, 2009). After accounting for PCR duplicates (removed using the Picard software: http://picard.sourceforge.net) and reads that did not align to captured regions of the reference genome, the average coverage for these three samples was ~71x and each sample had >95% of the bases covered. A base within the 37.8Mb captured region was defined as covered if ≥5 short-reads spanned this nucleotide (Table S10).

Genetic differences between each patient genome and the reference genome were identified using the SAMtools variant calling program(Li et al., 2009) which identifies both single nucleotide variants (SNVs) and small insertion-deletions (indels). We then used the SequenceVariantAnalyzer software (SVA) (Ge et al., 2011) to annotate all identified variants. SVA was also used to apply quality control filters to the variants identified by SAMtools. High quality SNVs were obtained using the following criteria: consensus score ≥20, SNP quality score ≥20, and reads supporting SNP ≥3. High quality indels were obtained using the following criteria: consensus score ≥20, indel quality score ≥50, ratio of (reads supporting variant/reads supporting reference): 0.2–5.0, and reads supporting indel ≥3.

Exome sequencing in families C & D—The exomes of one of the individuals of family C (II.3) and four individuals of family D (II.1, II.2, II.4, II.5) were captured using the Agilent SureSelect all exon kit V3 (approximately 51.9 Mb of target sequences), and then sequenced in pair-ends (2x100 bp) on the Illumina HiSeq2000 (v3 chemistry; 3 exomes/lane format) at the McGill University Genome Quebec Innovation Center (Montreal, Canada). The sequences were aligned and the variants were called using GATK (Depristo et al., 2011). After removal of duplicate reads, using Picard, we obtained an average coverage of >80x per target base, with 95% of the target bases being covered at ≥10x. Only variants that meet all the following criteria were considered: Base coverage ≥8x, reads supporting the variant ≥3, ratio of reads supporting variant/reads supporting reference ≥20%. Variants were then annotated using Annovar(Wang et al., 2010).

Genotyping p. F362V

Genotyping of the p.F362V variant in 1,160 controls was performed in the Center for Human Genome Variation at Duke University (Durham, NC). This was done using a custom TaqMan genotyping assay (Applied Biosystems, Foster City, CA): Forward: 5′-CCT GCG TAA GTT CAT CTG ATC CTT -3′ Reverse: 5′-GTA TAT TCG GAA GAA CAC AGA TAG CGT -3′ Probe: 5′-TCC AGA GA[A/C] GAT CAC C-3′.

Genotyping of the p.F362V variant in 80 Iranian Jewish controls and the non-exome-sequenced family members (Figure 1: Family A: I-1, I-2, II-2, II-3, II-4 and Family B: I-1, I-2, II-1) was performed at the Gertner Institute of Human Genetics, Sheba Medical Center, Israel. Sanger Sequencing (Figure 1B) or restriction digest with the restriction enzyme, Alw26I (data not shown) were used to perform this genotyping. Both methods used the following custom primer sequences: Forward: 5′-CTT TCA ATT ATT TCC AAA AAT CAA ATC -3′ and Reverse 5′-CAC TGT CAT ACT GAA AGA TGA TAG AAA -3′. These primers resulted in a 286bp amplicon that targeted the nucleotide of interest.

The p.F362V variant, found in families A and B, was validated in these three samples using all three methods: TaqMan genotyping, Sanger sequencing, and restriction digestion.

Genotyping p.R550C and p.A6E in French Canadian and Bangladeshi controls

Sanger sequencing of PCR amplified products was used to genotype p.R550C and p.A6E variants. The following custom primers were used for p.A6E: Forward: 5′-GCC GGT TGA ATG TAG AGG TC -3′ and Reverse: 5′-CCA AAG CAG CAG TTG GTG TA -3′. The following custom primers were used for p.R550C: Forward: 5′-GCC ATT TTA AGC CAT TTT GC -3′ and Reverse: 5′-TTT CCC TTT TCC TAG CTT ACC C -3′. The mutations p.R550C and p.A6E were genotyped in 300 French Canadian healthy controls. In addition, p.R550C was genotyped in 225 Bangladeshi healthy controls.

Clone preparations

Full-length cDNA encoding human *ASNS* was amplified from first-strand cDNA derived from the HEK-293 human kidney cell line with an RNeasy plus mini kit (QIAGEN, Santa Clarita, CA), High Capacity cDNA Reverse Transcription Kit (Applied Biosystems, Foster city, CA), Phusion HF DNA polymerase (Finnzymes, Espoo, Finland), and a specific primer set (5′-CTC GAG ATG TGT GGC ATT TGG GCG CT -3′ and 5′-CTC GAG CCT AAG CTT TGA CAG CTG ACT -3′). The cDNA was subcloned into the pCR-Blunt II-TOPO vector (Invitrogen-Life Technologies, Carlsbad, CA, USA) and subjected to sequence analysis (pCR-Blunt II-ASNS-WT). Using pCR-Blunt II-ASNS-WT, A6E, F362V, and R550C of *ASNS* were made by PCR-directed mutagenesis using Phusion HF DNA polymerase and a specific primer set (A6E: 5′-GCT GTT TGG CAG TGA TGA TTG -3′ and 5′-TCC CAA ATG CCA CAC ATC TC -3′; F362V: 5′-GTC TCT GGA GAA GGA TCA GA -3′ and 5′-GAT CAC CAC GCT ATC TGT GT -3′; R550C: 5′-GCA CGC TGA CCC ACT AC -3′ and 5′-AGG CAG AAG GGT CAG TGC -3′) which were phosphorylated by T4 polynucleotide kinase (NEW ENGLAND BioLabs, Ipswich, MA). The amplicons were self-ligated using T4 DNA ligase (Promega, Madison, WI) and subjected to sequence analysis (pCR-Blunt II-ASNS-A6E, pCR-Blunt II-ASNS-F362V, and pCR-Blunt II-ASNS-R550C). *ASNS* human cDNA containing each allele was subcloned into the pcDNA3.1(+) vector (Invitrogen-Life Technologies) using the KpnI and XbaI sites from pCR-Blunt II-ASNS-WT, pCR-Blunt II-ASNS-A6E, pCR-Blunt II-ASNS-F362V, or pCR-Blunt II-ASNS-R550C and subjected to sequence analysis (pcDNA3.1(+)-ASNS-WT, pcDNA3.1(+)-ASNS-A6E, pcDNA3.1(+)-ASNS-F362V, or pcDNA3.1(+)-ASNS-R550C; Figure S2).

Using pcDNA3.1(+)-ASNS-WT, pcDNA3.1(+)-ASNS-A6E, pcDNA3.1(+)-ASNS-F362V, or pcDNA3.1(+)-ASNS-R550C, FLAG-tagged modified ASNS were made by two-step PCR-directed mutagenesis using Phusion HF DNA polymerase and specific primer sets (first step: 5′-GAC AAG TAG GCT CGA GAA GGG -3′ and 5′-GTA GTC AGC TTT GAC AGC TGA C -3′; second step: 5′-GAC GAT GAC AAG TAG GCT CGA GAA GGG -3′ and 5′-GTC CTT GTA GTC AGC TTT GAC AG -3′) which were phosphorylated by T4 polynucleotide kinase, the amplicons were self-ligated using T4 DNA ligase, and subjected to sequence analysis (pcDNA3.1(+)-ASNS-FLAG-WT, pcDNA3.1(+)-ASNS-FLAG-A6E, pcDNA3.1(+)-ASNS-FLAG-F362V, or pcDNA3.1(+)-ASNS-FLAG-R550C). cDNAs encoding FLAG-tagged human ASNS were subcloned into pcDNA3.1(+) vector again, using the KpnI and XbaI sites and subjected to sequence analysis (Figure S2).

Cell culture: RT-PCR

Empty pcDNA3.1 (+) vector, pcDNA3.1(+)-ASNS wild type or pcDNA3.1(+)-ASNS mutant (p.F362V, p.R550C, or p.A6E) were transfected into the monkey COS-7 kidney cell line or human HEK-293 kidney cells by lipofection using Lipofectamine 2000 (Invitrogen-Life Technologies). Total RNA was extracted from transfectants using an RNeasy plus mini kit, and first-strand full-length cDNA encoding human ASNS was synthesized using the High Capacity cDNA Reverse Transcription Kit (Applied Biosystems, Foster city, CA). RT

PCR to detect ASNS mRNA expression was performed in 25 cycles at 96°C for 30 sec, 60°C for 30 sec, and 72°C for 30 sec using AmpliTaq Gold DNA polymerase (Applied Biosystems) and a specific primer set (5′-TGC ACG CCC TCT ATG ACA AT -3′ and 5′-CAC CTT TCT AGC AGC CAG TA -3′) (Figure 3A).

Cell culture: Western blotting

Forty eight hours after transfection the cells were lysed with RIPA buffer (Sigma-Aldrich, St. Louis, MO) with Protease inhibitor cocktail (Sigma-Aldrich), and the lysates were subjected to SDS PAGE gel and transferred to a polyvinylidene difluoride membrane (Millipore, Billerica, MA). The membranes were incubated with anti-FLAG M2 monoclonal antibody (Sigma-Aldrich, St. Louis, MO), or anti-actin antibody (Santa Cruz Biotechnology, Dallas, Texas). Proteins were visualized with the ECL plus western blotting detection system (GE Healthcare, Piscataway, NJ). For Leupeptin treatment, 24 h post-transfection, the cells were incubated with 100μM Leupeptin (Sigma Aldrich). After 8h incubation with Leupeptin, the cells were lysed, and FLAG-tagged ASNS were detected as above.

Protein conservation

Species and ASNS proteins were from: gi P08243 (Human, *Homo sapiens)*, ENSMUSP00000031766 (mouse, *Mus Musculus*), ENSGALP00000015846, (chicken, *Gallus gallus)*, ENSACAP00000012780 (Lizard, *Anolis carolinensis*), ENSXETP00000054608, (Frog, *Xenopus tropicalis)*, ENSTRUP00000013503 (Fish, Fugu, *Takifugu rubripe*), FBpp0089009 (Fruitfly, *Drosophila melanogaster*), NP_741864 (worm, nematode *Caenorhabditis elegans*), YGR124W (yeast, *Saccharomyces cerevisia*) and YP_003233213.1 (bacterium, *Escherichia coli*) (Figure 4A). Sequence alignment was performed using ClustalW(Thompson et al., 2002), and alignment editing with the BioEdit software (http://www.mbio.ncsu.edu/bioedit/bioedit.html).

The pdb structure was made using Discovery Studio program (http://accelrys.com/products/discovery-studio/) (Figure 4B).

Mouse analyses

Asns mice were obtained from the Eucomm consortium. Mice were maintained by breeding to C57BL/6NTac. Histology at P0 was performed by cryopreservation of tissue, cryosectioning, and hematoxylin and eosin staining. Histology in adult brains was performed by fixation of tissue using formalin perfusion. Tissue was sent to Histoserv.com (Gaithersburg, MD) for paraffin embedding, sectioning and staining. Analysis of area and thickness was performed by quantifying measurements using ImageJ. The p-values for structural measurements were obtained using an unpaired t-test and calculations were done using R.

cDNA

Mouse cerebral hemispheres were carefully dissected. Total RNA was extracted from brain tissue using an RNeasy plus mini kit, and first-strand full-length cDNA encoding human ASNS was synthesized using the High Capacity cDNA Reverse Transcription Kit (Applied Biosystems, Foster city, CA).

Quantitative real-time RT-PCR

Quantitative real-time PCR was done using a *Asns* gene expression assay, with FAM reporter, spanning exons 7–8 (Mm00803785_m1; Life Technologies, Carlsbad, California) and a *Gapdh* gene expression assay with VIC reporter (Mm99999915_g1; Life Technologies, Carlsbad, California). Samples were run in triplicate and the standard curve

was made using cDNA from a non-test wild type sample. Twelve mice between three and four months of age were used for qPCR. Four mice of each genotype were used ($Asns^{+/+}$, $Asns^{+/-}$, $Asns^{-/-}$). One-way analysis of variance (ANOVA) was used to assess expression differences between the three genotypes ($P<0.00001$). A post-hoc two-tailed t-test was then used to assess genotypic differences in expression ($P_{WT\text{-}Asns^{+/-}}=0.00001$, $*P_{WT\text{-}Asns^{-/-}}<0.00001$, $*P_{Asns^{+/-}\text{-}Asns^{-/-}}=0.00083$).

Regular RT-PCR—RT PCR to detect *Asns* mRNA expression was performed in 35 cycles at 96°C for 30 sec, 58°C for 30 sec, and 72°C for 90 sec using AmpliTaq Gold DNA polymerase (Applied Biosystems) and a specific primer set (5′-CAG TGT CTG AGT GCG ATG AAG A -3′ and 5′-GCG TTC AAA GAT CTG ACG GTA G-3′) (Figure S4).

RT PCR to detect *Gapdh* mRNA expression was performed in 25 cycles at 96°C for 30 sec, 57°C for 30 sec, and 72°C for 45 sec using AmpliTaq Gold DNA polymerase (Applied Biosystems) and a specific primer set (5′-ACC ACA GTC CAT GCC ATC AC-3′ and 5′-CAC CAC CCT GTT GCT GTA GCC-3′) (Figure S4).

Western blotting—Two different antibodies were tried for detection of mouse Asns: anti-human-ASNS which recognizes amino acid residues 506–520 of ASNS (Sigma-Aldrich) and anti-Asns, with species reactivity in mouse, rat, and human, which recognizes amino acid residues at the C-terminus (Abcam). Both were nonspecific (data not shown).

Video-EEG recordings of mice—Two adult *Asns* homozygous and one age-matched wild-type (*WT*) mice were anesthetized by intraperitoneal injection of Nembutal (60mg/kg). Under stereotaxic guidance, four monopolar electrodes were implanted into the subdural space over the left and right parietal cortex and occipital cortex for chronic electroencephalographic (EEG) recording. After a 7-day postoperative recovery, EEG activity was recorded with the mouse moving freely in a cage for 80 hours; animal behavior was recorded simultaneously with a digital video camera. The EEG and behavioral activities were analyzed by an individual blinded to mouse genotype.

Supplementary Material

Refer to Web version on PubMed Central for supplementary material.

Acknowledgments

We would like to thank all four families for their willingness to participate in this study. J.L. Michaud is a National Scientist of the Fonds de Recherche du Québec - Santé. E.K. Ruzzo is funded by a pre-doctoral grant from the Epilepsy Foundation and the Jo Rae Wright Fellowship for outstanding women in science (Duke University). J.M. Capo-Chichi holds a salary award from the Réseau de Médecine Génétique Appliquée du Québec (RMGA). We acknowledge the following colleagues for supplying control samples: R. Brown, G. Cavalleri, L. Cirulli, N. Delanty, C. Depondt, V. Dixon, E. Heinzen, J. Hoover-Fong, A. Husain, D. Levy, K. Linney, W. Lowe, J. McEvoy, M. Mikati, J. Milner, A. Need, R. Ottman, R. Radtke, J. Silver, M. Silver, S. Sisodiya, N. Sobriera, D. Valle, and N. Walley. We wish to thank Katherine Whang for helping to section the mouse brains. We wish to thank C. Means and T. Rhodes for helping with the behavioral experiments; and J. Zhou and C. Elms for breeding, genotyping, and maintaining the mice. We thank R. Olender and P. Allard for helpful insights. We also thank the members of the RMGA bioinformatic team (Alexandre Dionne-Laporte, Dan Spiegelman, Edouard Henrion, and Ousmane Diallo) for the bioinformatic analysis of the exome sequencing data (families C and D). This research has been funded in part by federal funds from the Center for HIV/AIDS Vaccine Immunology (“CHAVI”) under a grant from the National Institute of Allergy and Infectious Diseases, National Institutes of Health, Grant Number UO1AIO67854 to D.B. Goldstein, and by the March of Dimes (grant no. 12-FY10-236) and Canadian Institutes of Health Research (MOP 106499) to J.L. Michaud. Additional funding provided by: ARRA 1RC2NS070342-01, NIMH Grant RC2MH089915, NINDS Award# RC2NS070344, and the Crown Human Genome Center at the Weizmann Institute of Science.

References

Adams DJ, van der Weyden L. Contemporary approaches for modifying the mouse genome. Physiological Genomics. 2008; 34:225–238. [PubMed: 18559964]

Adzhubei IA, Schmidt S, Peshkin L, Ramensky VE, Gerasimova A, Bork P, Kondrashov AS, Sunyaev SR. A method and server for predicting damaging missense mutations. Nat Meth. 2010; 7:248–249.

Akiyama T, Kobayashi K, Higashikage A, Sato J, Yoshinaga H. CSF/plasma ratios of amino acids: Reference data and transports in children. Brain Dev. 2012:1–7.

Ayoub AE, Oh S, Xie Y, Leng J, Cotney J, Dominguez MH, Noonan JP, Rakic P. Transcriptional programs in transient embryonic zones of the cerebral cortex defined by high-resolution mRNA sequencing. Proceedings of the National Academy of Sciences. 2011; 108:14950–14955.

Bond J, Roberts E, Mochida GH, Hampshire DJ, Scott S, Askham JM, Springell K, Mahadevan M, Crow YJ, Markham AF, et al. ASPM is a major determinant of cerebral cortical size. Nat Genet. 2002; 32:316–320. [PubMed: 12355089]

Chen H. Amino Acid Deprivation Induces the Transcription Rate of the Human Asparagine Synthetase Gene through a Timed Program of Expression and Promoter Binding of Nutrient-responsive Basic Region/Leucine Zipper Transcription Factors as Well as Localized Histone Acetylation. Journal of Biological Chemistry. 2004; 279:50829–50839. [PubMed: 15385533]

de Koning TJ. PART 8: AMINO ACIDS. The Online Metabolic & Molecular Bases of Inherited Disease. 2013:1–14.

Depristo MA, Banks E, Poplin R, Garimella KV, Maguire JR, Hartl C, Philippakis AA, Del Angel G, Rivas MA, Hanna M, et al. A framework for variation discovery and genotyping using next-generation DNA sequencing data. Nat Genet. 2011; 43:491–498. [PubMed: 21478889]

Ge D, Ruzzo EK, Shianna KV, He M, Pelak K, Heinzen EL, Need AC, Cirulli ET, Maia JM, Dickson SP, et al. SVA: software for annotating and visualizing sequenced human genomes. Bioinformatics. 2011; 27:1998–2000. [PubMed: 21624899]

Greco A, Gong S, Ittmann M, Basilico C. Organization and expression of the cell cycle gene, ts11, that encodes asparagine synthetase. Molecular and Cellular Biology. 1989; 9:2350. [PubMed: 2569668]

Häberle J, Görg B, Rutsch F, Schmidt E, Toutain A, Benoist JF, Gelot A, Suc AL, Höhne W, Schliess F, et al. Congenital glutamine deficiency with glutamine synthetase mutations. N Engl J Med. 2013; 353:1926–1933. [PubMed: 16267323]

Häberle J, Shahbeck N, Ibrahim K, Schmitt B, Scheer I, O'Gorman R, Chaudhry FA, Ben-Omran T. Glutamine supplementation in a child with inherited GS deficiency improves the clinical status and partially corrects the peripheral and central amino acid imbalance. Orphanet Journal of Rare Diseases. 2012; 7:48–48. [PubMed: 22830360]

Hongo S, Chiyo T, Takeda M. Cloning of cDNA for asparagine synthetase from rat Sertoli cell. Biochem Mol Biol Int. 1996; 38:189–196. [PubMed: 8932534]

Hubbard TJP, Aken BL, Ayling S, Ballester B, Beal K, Bragin E, Brent S, Chen Y, Clapham P, Clarke L, et al. Ensembl 2009. Nucleic Acids Res. 2009; 37:D690–D697. [PubMed: 19033362]

Jackson AP, Eastwood H, Bell SM, Adu J, Toomes C, Carr IM, Roberts E, Hampshire DJ, Crow YJ, Mighell AJ, et al. Identification of microcephalin, a protein implicated in determining the size of the human brain. The American Journal of Human Genetics. 2002; 71:136–142.

Li B, Gu L, Luo C, Li W, Jiang L, Shen S, Jiang H, Zhang B, Chen J, Xue H. The downregulation of asparagine synthetase expression can increase the sensitivity of cells resistant to L-asparaginase. Leukemia. 2006; 20:2199–2201. [PubMed: 17039232]

Li H, Durbin R. Fast and accurate short read alignment with Burrows-Wheeler transform. Bioinformatics. 2009; 25:1754–1760. [PubMed: 19451168]

Li H, Handsaker B, Wysoker A, Fennell T, Ruan J, Homer N, Marth G, Abecasis G, Durbin R. 1000 Genome Project Data Processing Subgroup. The Sequence Alignment/Map format and SAMtools. Bioinformatics. 2009; 25:2078–2079. [PubMed: 19505943]

Mahmood S, Ahmad W, Hassan MJ. Autosomal recessive primary microcephaly (MCPH): clinical manifestations, genetic heterogeneity and mutation continuum. Orphanet Journal of Rare Diseases. 2011; 6:39. [PubMed: 21668957]

Nachman MW, Crowell SL. Estimate of the mutation rate per nucleotide in humans. Genetics. 2000; 156:297–304. [PubMed: 10978293]

Ng PC, Henikoff S. SIFT: Predicting amino acid changes that affect protein function. Nucleic Acids Res. 2003; 31:3812–3814. [PubMed: 12824425]

Nishimura F, Nishihara M, Mori M, Torii K, Takahashi M. Excitability of neurons in the ventromedial nucleus in rat hypothalamic slices: modulation by amino acids at cerebrospinal fluid levels. Brain Research. 1995; 691:217–222. [PubMed: 8590056]

Pulvers JN, Bryk J, Fish JL, Wilsch-Bräuninger M, Arai Y, Schreier D, Naumann R, Helppi J, Habermann B, Vogt J, et al. Mutations in mouse Aspm (abnormal spindle-like microcephaly associated) cause not only microcephaly but also major defects in the germline. Proceedings of the National Academy of Sciences. 2010; 107:16595–16600.

Richards NGJ, Kilberg MS. Asparagine Synthetase Chemotherapy. Annu Rev Biochem. 2006; 75:629–654. [PubMed: 16756505]

Scholl-Burgi S, Haberlandt E, Heinz-Erian P, Deisenhammer F, Albrecht U, Sigl SB, Rauchenzauner M, Ulmer H, Karall D. Amino Acid Cerebrospinal Fluid/Plasma Ratios in Children: Influence of Age, Gender, and Antiepileptic Medication. Pediatrics. 2008a; 121:e920–e926. [PubMed: 18332074]

Scholl-Burgi S, Haberlandt E, Heinz-Erian P, Deisenhammer F, Albrecht U, Sigl SB, Rauchenzauner M, Ulmer H, Karall D. Amino Acid Cerebrospinal Fluid/Plasma Ratios in Children: Influence of Age, Gender, and Antiepileptic Medication. Pediatrics. 2008b; 121:e920–e926. [PubMed: 18332074]

Thompson JD, Gibson TJ, Higgins DG. Multiple sequence alignment using ClustalW and ClustalX. Curr Protoc Bioinformatics. 2002; Chapter 2(Unit2.3)

Visel A, Thaller C, Eichele G. GenePaint.org: an atlas of gene expression patterns in the mouse embryo. Nucleic Acids Res. 2004; 32:D552–D556. [PubMed: 14681479]

Wang K, Li M, Hakonarson H. ANNOVAR: functional annotation of genetic variants from high-throughput sequencing data. Nucleic Acids Res. 2010; 38:e164–e164. [PubMed: 20601685]

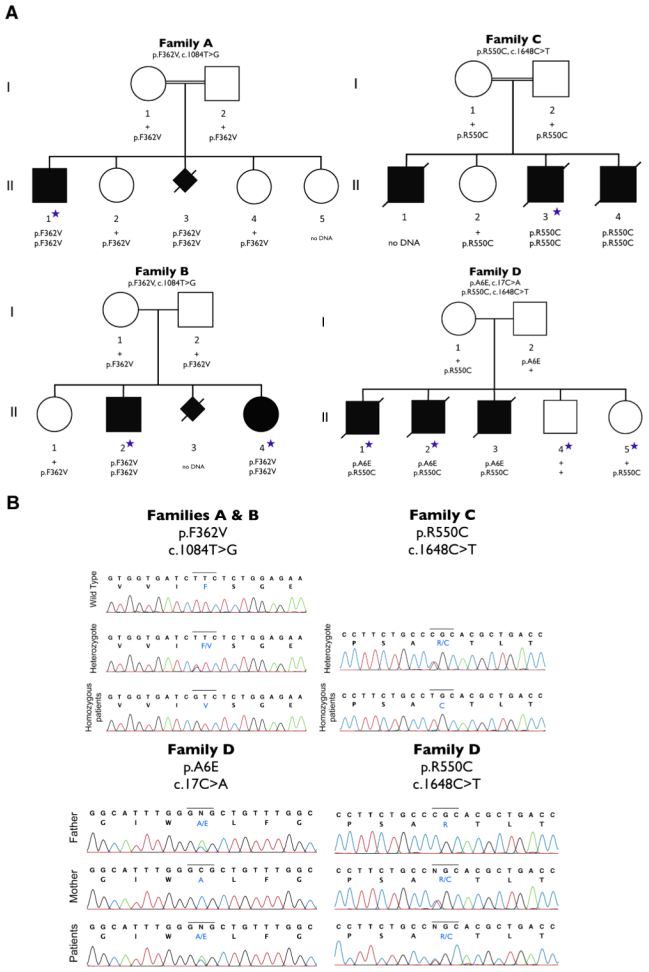

Figure 1. Four families with *ASNS* mutations

A. Cosegregation of mutations within each of the four families. Filled symbols represent known or presumed (in the case of aborted fetus) affected individuals. The individuals with a blue star were exome-sequenced.

B. Sanger sequencing confirmation for all three *ASNS* mutations in the four families. For family D, Sanger sequencing also confirmed inheritance of each mutation from a different parent (compound heterozygote).

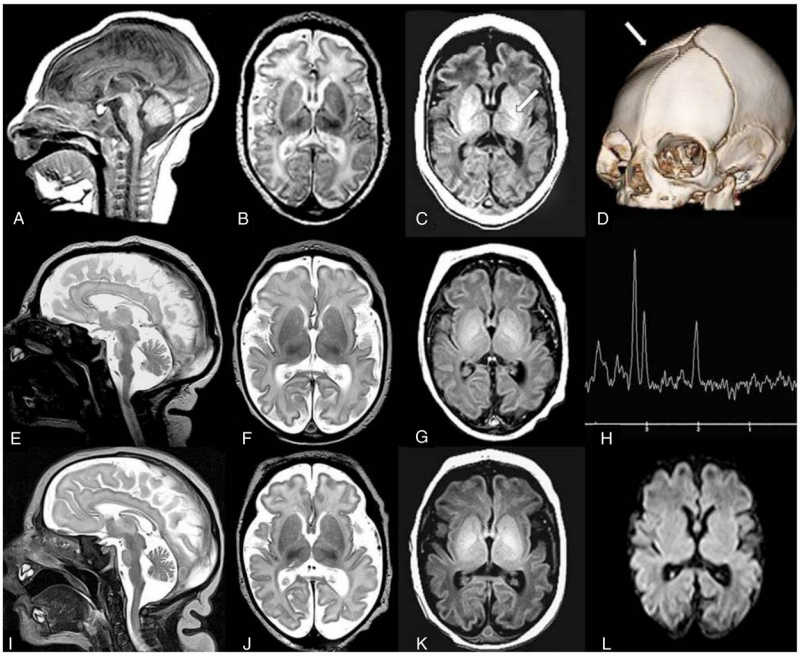

Figure 2. MRI images from family C

Sibling C.II.1 (A–D): Sagittal T1W image (A) performed at 13 days of age reveals decreased size of pons. Axial T2W image (B) reveals prominent pericerebral fluid spaces surrounding the brain due to volume loss. White matter is diffusely higher in signal intensity than the cortical ribbon, suggesting delayed myelination. Axial T1W image (C) confirms lack of bright myelin stripe in the posterior limb of internal capsule (arrow). Three-D CT (D) at two months of age confirms ridge (arrow) from overlapping sutures, palpable at birth. DNA confirmation was not obtained in this infant.

Sibling C.II.3 (E–H): Sagittal T2W image (E) performed at six days of age reveals decreased size of pons. Axial T2W image (F) demonstrates prominent pericerebral fluid spaces surrounding the brain due to volume loss. Axial T1W image (G) confirms lack of myelin stripe in posterior limb of the internal capsule (PLIC). Magnetic resonance spectroscopy (MRS) TE144 (H) performed in the basal ganglia is age appropriate (as it was in all 3 siblings).

Sibling C.II.4 (I–L): Sagittal T2W image (I) performed at one day of age reveals decreased size of pons. Axial T2W image (J) confirms pericerebral fluid prominence due to cerebral volume loss in a manner similar to siblings. Axial T1W image (K) shows lack of myelin stripe in PLIC. Diffusion weighted imaging (DWI) (L) is normal (as it was in all 3 siblings). *See also* Figure S1.

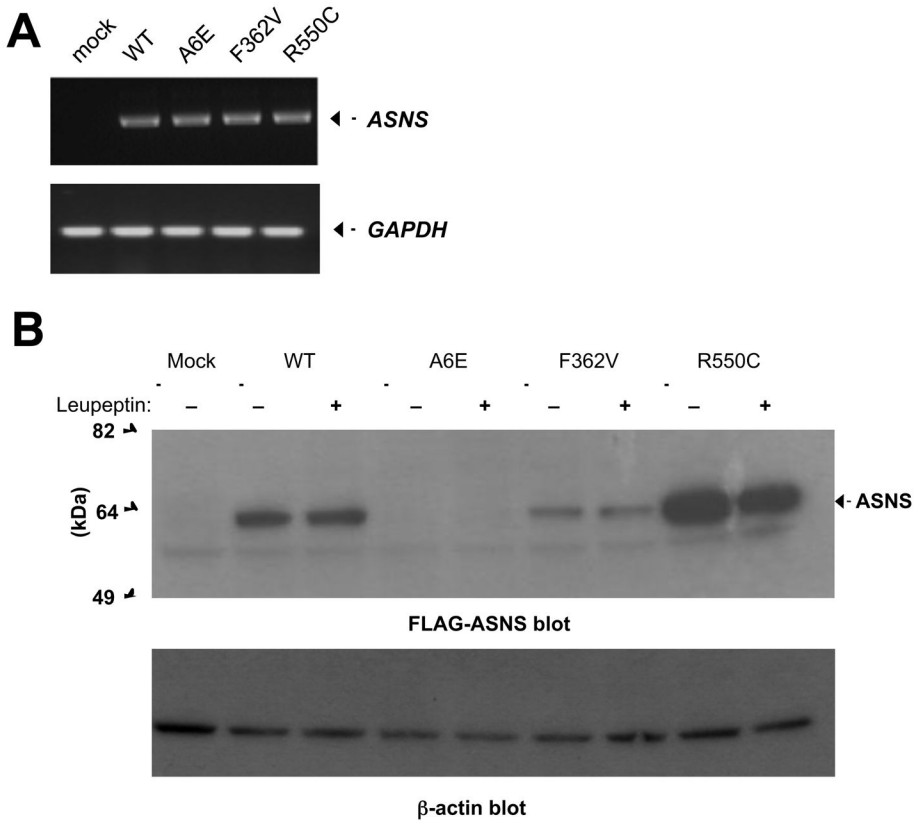

Figure 3. Functional impact of *ASNS* mutations

A. RT-PCR to detect *ASNS* mRNA expression in COS-7 cells transfected with empty, wild-type, or mutant vectors.

B. Western Blots detecting ASNS-FLAG protein abundance, with or without Leupeptin treatment, in the HEK293 transfectants using an anti-FLAG antibody. β-actin was used as a loading control.

See also Figure S2.

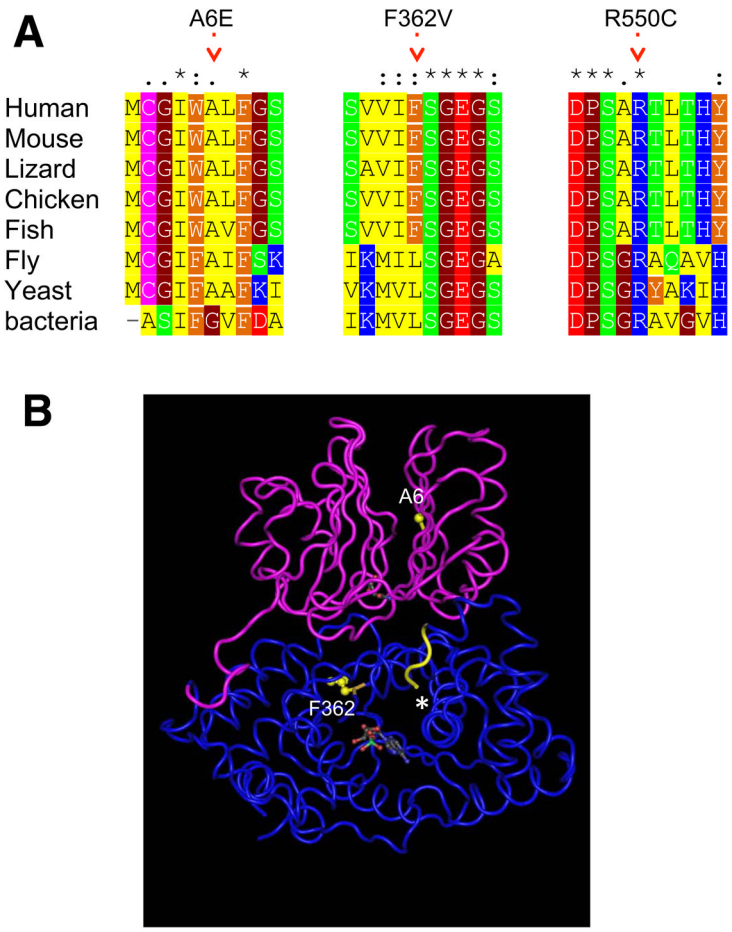

Figure 4. Location and conservation of mutated residues in the *ASNS* gene

A. A multiple alignment of human ASNS and selected orthologs. Only the regions harboring mutations are shown. On top: * - identical position, : - conserved substitutions, . - semi-conserved substitution. Color code is for amino acid type: red=negative, blue=positive, green=polar, yellow=aliphatic, orange=aromatic, brown=helix breaker.

B. The structure of *E. coli* glutamine dependent asparagine synthetase B (protein databank ID 1CT9), a bacterial ortholog of human ASNS (Figure 4A). The N-terminal glutamine amidotransferase domain is colored in pink, and the C-terminal asparagine synthase domain is colored in blue. The residues inferred to be equivalent to the mutated A6E and F362V are highlighted in yellow and the approximate location of the mutated R550C is shown with an asterisk (crystallography could not be determined for the distal end of C-terminal domain). Also, the AMP and glutamine molecules are shown in space-filling style.

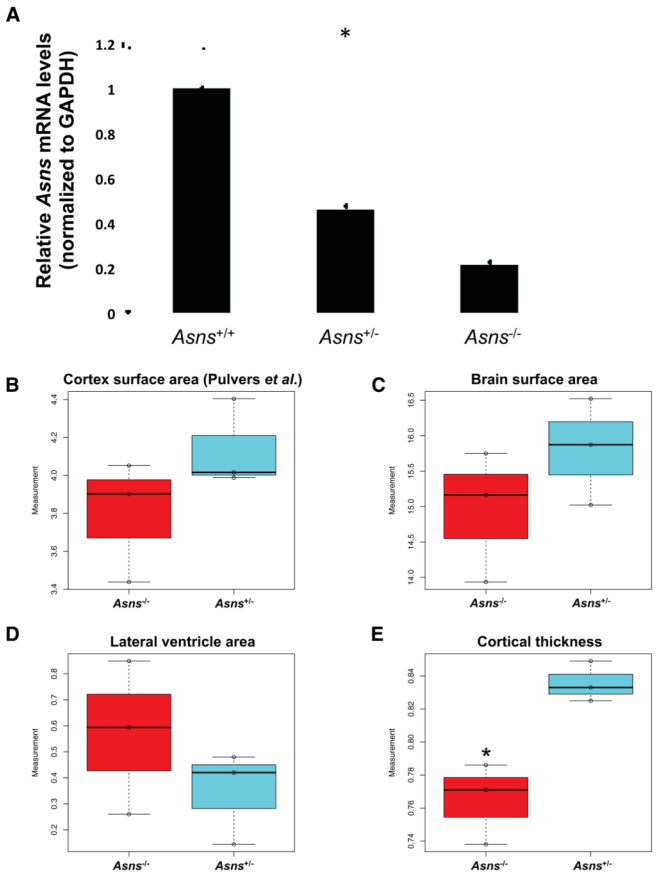

Figure 5. Asns deficient mice and structural brain abnormalities

A. Detection of *Asns* mRNA (qRT-PCR) in the mouse brain. Four mice of each genotype were used (all between three and four months of age). The expression differences between the three genotypes are significant (*one-way ANOVA test P<0.00001). A post-hoc two-tailed t-test revealed both mutant genotypes were significantly different from wild type expression ($P_{WT\text{-}ASNS(+/-)}$ =0.00001, *$P_{WT\text{-}ASNS(-/-)}$<0.00001) and significantly different from each other (*$P_{ASNS(+/-)\text{-}ASNS(-/-)}$=0.00083). Error bars represent SEM.

B–E. Measurements of adult mouse brain (P84) coronal sections, analyzed using Image J software(Rasband, 2008), comparing three homozygous mutants to heterozygous littermates. (B) Cortical surface area as measured in Pulvers *et al.* 2010. (C) Surface area of the left hemisphere of the brain section, (D) surface area of the lateral ventricle in the left hemisphere of the brain section, and (E) cortical thickness, measured from the edge of the hippocampus to the outer cortex. Asterisk (*) indicates a significant difference by an unpaired t-test (P=0.022).

See also Figures S3, S4, and S5.

Table 1

Clinical features of patients with mutations in *ASNS*

	Family A	Family B		Family C			Family D		
Consanguinity	**yes**	**no**		**yes**			**no**		
Ethnic origin	**Iranian Jews**	**Iranian Jews**		**Bangladeshi**			**French Canadian**		
Subjects	**A.II.1**	**B.II.2**	**B.II.4**	**C.II.1**	**C.II.3**	**C.II.4**	**D.II.1**	**D.II.2**	**D.II.3**
Genotype	p.F362V/p.F362V	p.F362V/p.F362V	p.F362V/p.F362V	Not determined	p.R550C/p.R550C	p.R550C/p.R550C	p.A6E/p.R550C	p.A6E/p.R550C	p.A6E/p.R550C
Gender	Male	Male	Female	Male	Male	Male	Male	Male	Male
Age	14 y	14 y	12 y	4 mo†	3 mo†	6 mo†	9 days†	11 mo†	12 mo†
HC[1] at birth (cm)	31.5 (−2.5SD)	31 (−3SD)	31 (−2SD/−3SD)	30.5 (−3.5SD)	33 (−1SD/−2SD)	32 (−2SD)	31.5 (−2.5SD)	31 (−3SD)	28.5 (−1SD/−2SD)[2]
Developmental delay	severe	severe	severe	severe	severe	severe	severe	severe	severe
Progressive microcephaly	yes	yes	yes	yes	yes	yes	NA	yes	yes
Epilepsy									
age at onset	1 mo	2 wks	3 wks	none	none	none	4 days	9 mo[5]	8 days
type of seizures	spasms, tonic, myoclonic, GTC[3]	spasms, tonic, myoclonic, GTC[3]	spasms, tonic, myoclonic, GTC[3]	none	none	none	tonic, orobuccal	partial complex	partial complex
EEG pattern	hypsarrythmia, MISF[4]	hypsarrythmia, MISF[4]	hypsarrythmia, MISF[4]	disorganized background	disorganized background	disorganized background	NA	suppression bursts, MISF	suppression bursts, MISF
Clinical examination									
axial hypotonia	no	no	no	no	yes	yes	yes	yes	yes
appendicular hypertonia	yes	yes	yes	yes	yes	yes	yes	yes	yes
hyperreflexia	yes	yes	yes	yes	yes	yes	yes	yes	yes
hyperekplexia	no	no	no	yes	yes	yes	no	no	no
Brain MRI									
decreased cerebral volume	yes	yes	yes	yes	yes	yes	yes	yes	yes
decreased size of pons	no	no	no	yes	yes	yes	yes	yes	yes
simplified gyri	no	no	no	yes	yes	yes	yes	yes	yes

†deceased;

[1]head circumference;

[2]born at 33.5 weeks of gestation;

[3] generalized tonic-clonic seizures;

[4] multiple independent spike foci;

[5] tremulous movements and abnormal EEG at 4 days; partial complex seizures with eye deviation and focal epileptic activity at 9 months.

Table 2

Mutations identified in *ASNS*.

Nucleotide and amino acid positions are based on the NCBI Reference sequences NM_183356.3 and NP_899199.2, respectively. *See also* Tables S1–S10.

Family	Genotype	ASNS modification	Nucleotide change	Ethnicity	Frequency in control in-house exomes/genomes	Frequency in ancestry-matched controls	PolyPhen-2	SIFT
A	homozygous	p.F362V	c.1084T>G	Iranian Jewish	0/261	1/80	damaging (0.95)	damaging (0.04)
B	homozygous	p.F362V	c.1084T>G	Iranian Jewish	0/261	1/80	damaging (0.95)	damaging (0.04)
C	homozygous	p.R550C	c.1648C>T	Bangladeshi	0/169	0/225	damaging (1.00)	damaging (0.01)
D	compound heterozyous	p.R550C	c.1648C>T	French Canadian	0/169	0/300	damaging (1.00)	damaging (0.01)
		p.A6E	c.17C>A		0/169	0/300	damaging (0.898)	deleterious (0.02)

Table 3

Measurements of amino acid concentrations in patient blood and urine

Data was not available for all fields in all patients (NA). The reference concentrations are indicated within parentheses. *See also* Table S11.

	Plasma amino acid levels (μmol/L)			Urine amino acid levels (μmol/mmol creatinine)		
	glutamine	**aspartate**	**asparagine**	**glutamine**	**aspartate**	**asparagine**
B.II.2	1250 (254–823)	18 (1–24)	57 (23–112)	382 (20–112)	36 (1–10)	21 (0–24)
B.II.4	1149 (254–823)	2 (1–24)	49 (23–112)	57 (20–112)	40 (1–10)	4 (0–24)
C.II.1	NA	7 (17–21)	NA	NA	NA	NA
C.II.3	NA	NA	12 (16–21)	NA	NA	NA
C.II.4	NA	12 (0–20)	NA	NA	NA	NA
D.II.1	439 (474–736)	7 (4–18)	11 (31–56)	NA	NA	NA
D.II.2	668 (474–736)	9 (4–18)	55 (31–56)	NA	NA	NA